

Spin-stress and spin-strain coupling in diamond-based hybrid spin oscillator systems

A. Barfuss, M. Kasperczyk, J. Kölbl, and P. Maletinsky*

Department of Physics, University of Basel, Klingelbergstrasse 82, CH-4056 Basel, Switzerland



(Received 20 September 2018; revised manuscript received 18 February 2019; published 8 May 2019)

Hybrid quantum systems, which combine quantum-mechanical systems with macroscopic mechanical oscillators, have attracted increasing interest as they are well suited as high-performance sensors or transducers in quantum computers. A promising candidate is based on diamond cantilevers, whose motion is coupled to embedded nitrogen-vacancy (NV) centers through crystal deformation. Even though this type of coupling has been investigated intensively in the past, several inconsistencies exist in available literature, and no complete and consistent theoretical description has been given thus far. To clarify and resolve these issues, we here develop a complete and consistent formalism to describe the coupling between the NV spin degree of freedom and crystal deformation in terms of stress, defined in the crystal coordinate system XYZ , and strain, defined in the four individual NV reference frames. We find that describing crystal deformation in XYZ significantly simplifies the formalism and therefore constitutes the preferred approach for future advances in the field. Furthermore, we illustrate how the developed formalism can be employed to extract values for the spin-stress and spin-strain coupling constants from data published by Teissier *et al.* [*Phys. Rev. Lett.* **113**, 020503 (2014)].

DOI: [10.1103/PhysRevB.99.174102](https://doi.org/10.1103/PhysRevB.99.174102)

I. INTRODUCTION

Hybrid systems combine quantum-mechanical two-level systems with macroscopic mechanical oscillators and have attracted increasing attention recently, largely with the goal of employing them as high-performance nanoscale sensors or transducers in multiqubit networks [1]. Such systems can furthermore serve as testbeds to study macroscopic objects in the quantum regime, provided the coupling between resonator motion and the two-level system resides in the high cooperativity regime [2]. An extensive variety of hybrid systems are already being studied. These include superconducting circuits coupled capacitively [3–6], ultracold atoms linked by radiation pressure forces [7–9], and quantum dots or solid-state spins coupled by magnetic field gradients [10–13] or crystal stress [14–18,28], to mechanical oscillators of different materials and shapes.

Hybrid spin-oscillator systems, in which the motion of a diamond resonator is coupled to the spin-degree of freedom of an embedded nitrogen-vacancy (NV) color center, are of particular interest [2]. The NV center provides a promising solid-state platform for quantum technologies due to its room-temperature operation with long spin coherence times [19] and well established optical methods for spin initialization and readout [20]. Diamond resonators benefit from the material's high Young's modulus, which provides excellent mechanical strength and gives rise to exceptional stress amplitudes per resonator displacement. Recent advances in diamond fabrication have further demonstrated high-quality resonators with quality factors $Q \sim 10^6$ [21–23]. Additionally, coupling between resonator and NV spin is intrinsic. Diamond-based hybrid systems thus come with minimized fabrication complexity and immediately offer a robust qubit-resonator link,

which is crucial for operating such systems in the quantum regime [24–26].

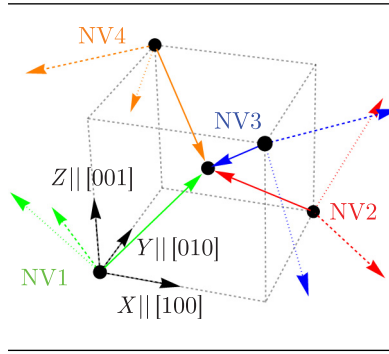
Consequently, the coupling between NV spin and crystal deformation has been explored in various experiments, starting with seminal work by Davies and Hamer, who investigated its influence on the NV's optical transitions in the 1970s [27]. Subsequent studies first aimed at probing the electronic level structure of NV ground and excited states [18,28–33], and recently started to investigate diamond-based hybrid spin-oscillator systems. Substantial evidence was found that quantum ground-state operation is in principle possible [17,18,28,34–38]. It was also discovered that crystal deformation allows for coherent control of the NV's spin degree of freedom [39,40] and that such hybrid systems can have future sensing applications, for example in protecting NV centers from environmental noise through dynamical decoupling [39,41,42] or as the main ingredient of spin-mechanical sensors for mass spectrometry and force microscopy [43].

Yet even though the coupling between NV spin and crystal deformation has been studied intensively, several differences and inconsistencies in its formal description exist in the published literature. Crystal deformation is treated in terms of stress [17,33,43,44] or strain [18,28,37], defined in crystal [33,43,44] or defect coordinate systems [17,18,28,37,45]. This already confusing situation is further complicated by inconsistent sign conventions for stress and strain [18,28,32,43], and the use of different, occasionally incorrect, interaction Hamiltonians in the literature. While recent works employ correct approximations of the complete interaction Hamiltonian [33,43], earlier studies rely on oversimplified versions where the tensorial nature of strain is neglected [17,18,28].

To clarify and resolve existing inconsistencies in the literature, we provide a complete and consistent theoretical treatment of the coupling between crystal deformation and the spin degree of freedom of negatively charged NV centers in the first part of this paper. To that end, we extend the available

*Corresponding author: patrick.maletinsky@unibas.ch

TABLE I. Definition and graphical representation of crystal (XYZ) and NV (xyz_k) coordinate systems employed in this work (for clarity, x axes are represented by dashed arrows, y axes by dotted arrows, and z axes by solid arrows). The given rotations \mathbf{K}_k with $k \in \{\text{NV2, NV3, NV4}\}$ describe a coordinate transformation of NV1 into NV2-4. $\mathbf{L}_{\text{NV1}} = \mathbf{R}_{[001]}(-3\pi/4)\mathbf{R}_{[\bar{1}10]}(-\alpha_{\text{NV}})$ represents the coordinate system transformation of $XYZ \rightarrow xyz_{\text{NV1}}$ with $\alpha_{\text{NV}} = \arccos(1/\sqrt{3})$. To obtain the rotations $\tilde{\mathbf{K}}_k$ in Kelvin notation, we replace all $\mathbf{R}_n(\theta)$ with $\tilde{\mathbf{R}}_n(\theta)$ (see Appendix B for definitions of rotation matrices in standard or Kelvin notation).



NV orientation	$\sqrt{2}\mathbf{e}_x$	$\sqrt{6}\mathbf{e}_y$	$\sqrt{3}\mathbf{e}_z$	\mathbf{K}_k	\mathbf{L}_k
NV1	$[\bar{1}10]$	$[\bar{1}\bar{1}2]$	$[111]$	$\mathbb{1}$	\mathbf{L}_{NV1}
NV2	$[1\bar{1}0]$	$[112]$	$[\bar{1}\bar{1}1]$	$\mathbf{R}_{[001]}(\pi)$	$\mathbf{L}_{\text{NV1}}\mathbf{K}_{\text{NV2}}$
NV3	$[110]$	$[1\bar{1}\bar{2}]$	$[\bar{1}1\bar{1}]$	$\mathbf{R}_{[010]}(\pi)$	$\mathbf{L}_{\text{NV1}}\mathbf{K}_{\text{NV3}}$
NV4	$[\bar{1}\bar{1}0]$	$[\bar{1}\bar{1}2]$	$[1\bar{1}\bar{1}]$	$\mathbf{R}_{[100]}(\pi)$	$\mathbf{L}_{\text{NV1}}\mathbf{K}_{\text{NV4}}$

work on spin-mechanical interaction [43,46] by illustrating in detail how to convert between strain, stress, crystal, or NV reference frames for all possible NV orientations. We demonstrate that the formalism is significantly simplified in many aspects, for example in the expressions for the induced level shifts or in terms of the necessary coordinate system definitions, if strain or stress tensors are defined within a crystal coordinate system XYZ as opposed to the case where they depend on the individual NV reference frames. In the second part, we illustrate how our formalism can be applied to relevant geometries and experimental settings of NV-based spin-mechanical coupling experiments. We derive the stress tensor in a singly clamped diamond cantilever under the influence of an external shear force. Subsequently, we use this stress tensor and the developed coupling formalism to quantify spin-mechanical coupling. In particular, we reanalyze experimental data from Teissier *et al.* [28] and correctly quantify the spin-stress coupling constants originally measured there.

II. SPIN-STRESS AND SPIN-STRAIN COUPLING IN THE NV $S = 1$ GROUND STATE

A. Employed coordinate systems

In this work, we choose a cubic reference frame with crystal coordinates XYZ , where $\mathbf{e}_X = (1, 0, 0)^T$, $\mathbf{e}_Y = (0, 1, 0)^T$, and $\mathbf{e}_Z = (0, 0, 1)^T$ (see Table I), in which diamond crystalline directions are defined. Owing to their axial symmetry, NV centers can have four different orientations in the diamond lattice. We therefore employ four NV reference frames xyz_k with $k \in \{\text{NV1, NV2, NV3, NV4}\}$. Each xyz_k is determined by a set of orthonormal basis vectors \mathbf{e}_i^k with $i \in \{x, y, z\}$, which are defined in Table I. Our choice of xyz_k is such that the z axes coincide with the symmetry axes (quantization axes) of the four defect orientations, and the y axes lie in NV symmetry planes. Defining the xyz_k with the x axes in the reflection planes is also common, but does not change the formalism we present in this work as the choice of the transverse axes does not affect the description as long as the quantization axis remains the same (see Appendix C). In the following, unless

noted otherwise, we refer to the NV frame for orientation NV1.

B. Spin-stress coupling expressed in crystal coordinates XYZ

The NV center consists of a substitutional nitrogen atom and a neighboring vacancy. In its orbital ground state, the negatively charged NV center forms an $S = 1$ spin system, with the spin sublevels $|0\rangle$, $|-1\rangle$, and $|+1\rangle$ being eigenstates of the spin operator S_z along the NV symmetry axis z (i.e., $S_z|m_s\rangle = m_s|m_s\rangle$). In the absence of symmetry-breaking fields, the electronic-spin states $|\pm 1\rangle$ are degenerate and shifted from $|0\rangle$ by a zero-field splitting $D_0 = 2.87$ GHz. An external magnetic field $\mathbf{B} = (B_x, B_y, B_z)^T$ induces a Zeeman splitting between the $|\pm 1\rangle$ spin states and in the presence of this field only, the NV spin is described by the Hamiltonian

$$H_0/h = D_0 S_z^2 + \gamma_{\text{NV}} \mathbf{B} \mathbf{S}, \quad (1)$$

where $\gamma_{\text{NV}} = 2.8$ MHz/G is the NV gyromagnetic ratio, h is Planck's constant, and $\mathbf{S} = (S_x, S_y, S_z)^T$ is the vector of the $S = 1$ spin matrices.

The coupling between crystal deformation and the NV spin can be explained by a stress-induced change to the spin-spin interaction, which arises from the distortion of the unpaired spin density [43]. The most general, symmetry-allowed spin-stress coupling Hamiltonian reads $H_\sigma = H_{\sigma 0} + H_{\sigma 1} + H_{\sigma 2}$, with

$$H_{\sigma 0}/h = M_z S_z^2, \quad (2a)$$

$$H_{\sigma 1}/h = N_x \{S_x, S_z\} + N_y \{S_y, S_z\}, \quad (2b)$$

$$H_{\sigma 2}/h = M_x (S_y^2 - S_x^2) + M_y \{S_x, S_y\}, \quad (2c)$$

where $\{S_i, S_j\} = (S_i S_j + S_j S_i)$ is the anticommutator and $M_{x,y,z}$ and $N_{x,y}$ are coupling amplitudes (see below) [46]. The term $H_{\sigma 0}$ preserves the NV symmetry and shifts $|\pm 1\rangle$ with respect to $|0\rangle$. In contrast, $H_{\sigma 2}$ leads to a coupling of spin sublevels $|\pm 1\rangle$, while $H_{\sigma 1}$ only has nonzero matrix elements between $|0\rangle$ and either $|-1\rangle$ or $|+1\rangle$. The stress-induced level shifts and splittings depend on NV orientation and are characterized by the five coupling

amplitudes [46,47]

$$M_x^{\text{NV1}} = b(2\sigma_{ZZ} - \sigma_{XX} - \sigma_{YY}) + c(2\sigma_{XY} - \sigma_{YZ} - \sigma_{XZ}), \quad (3a)$$

$$M_y^{\text{NV1}} = \sqrt{3}b(\sigma_{XX} - \sigma_{YY}) + \sqrt{3}c(\sigma_{YZ} - \sigma_{XZ}), \quad (3b)$$

$$M_z^{\text{NV1}} = a_1(\sigma_{XX} + \sigma_{YY} + \sigma_{ZZ}) + 2a_2(\sigma_{YZ} + \sigma_{XZ} + \sigma_{XY}), \quad (3c)$$

$$N_x^{\text{NV1}} = d(2\sigma_{ZZ} - \sigma_{XX} - \sigma_{YY}) + e(2\sigma_{XY} - \sigma_{YZ} - \sigma_{XZ}), \quad (3d)$$

$$N_y^{\text{NV1}} = \sqrt{3}d(\sigma_{XX} - \sigma_{YY}) + \sqrt{3}e(\sigma_{YZ} - \sigma_{XZ}) \quad (3e)$$

(given for NV orientation NV1). These further depend on the spin-stress coupling constants a_1, a_2, b, c, d, e and the stress tensor components σ_{IJ} [48,49]. Note that Eq. (3) is true for any stress tensor and therefore provides a powerful tool to predict the effect of spin-stress coupling. Moreover, we want to point out that owing to the axial symmetry of the system the coupling amplitudes from Eq. (3) are identical, regardless of whether the symmetry plane coincides with the xz or yz planes of the chosen NV reference frame [see Appendix C]. This greatly simplifies the formalism as different definitions of the NV frame yield the same results.

Before we include the remaining NV orientations NV2-4 in our formalism, we first briefly demonstrate how Hamiltonian (2) can be used to predict stress-induced level shifts in the $S = 1$ ground state. To that end, we consider a scenario in which no external magnetic field \mathbf{B} is applied. Under such conditions, the terms in $H_{\sigma 1}$ are far off resonance and can be neglected to first order, resulting in the stress-induced level shifts

$$\begin{aligned} \Delta_{|\pm 1\rangle} &= [E_{|\pm 1\rangle}(P) - E_{|\pm 1\rangle}(P = 0)]/\hbar \\ &= \left(M_z \pm \sqrt{M_x^2 + M_y^2}\right), \end{aligned} \quad (4)$$

where $E_{|\pm 1\rangle}(P)$ denote the energies of the new eigenstates in the $|\pm 1\rangle$ manifold with applied stress of amplitude P . For uniaxial stress acting along \mathbf{e}_P , the stress tensor components are

$$\sigma_{IJ} = P \cos(\angle \mathbf{e}_P \mathbf{e}_I) \cos(\angle \mathbf{e}_P \mathbf{e}_J), \quad (5)$$

where $\angle \mathbf{e}_P \mathbf{e}_I$ and $\angle \mathbf{e}_P \mathbf{e}_J$ denote the angles between the applied stress and the crystal axes \mathbf{e}_I and \mathbf{e}_J , with $I, J \in \{X, Y, Z\}$ [47]. Consequently, the resulting level shifts for stresses along the $[100]$, $[110]$, and $[111]$ directions are

$$\Delta_{|\pm 1\rangle}^{[100]}/P = a_1 \pm 2b, \quad (6a)$$

$$\Delta_{|\pm 1\rangle}^{[110]}/P = a_1 + a_2 \pm (b - c), \quad (6b)$$

$$\Delta_{|\pm 1\rangle}^{[111]}/P = a_1 + 2a_2. \quad (6c)$$

At this point it is important to realize that the four coupling constants a_1, a_2, b , and c are necessary to fully describe spin-stress coupling for vanishing \mathbf{B} . We also want to point out that an ambiguity persists with regard to the sign of the coupling constants b and c . This arises from the fact that stress-induced splittings in the $|\pm 1\rangle$ manifold are given by $(M_x^2 + M_y^2)^{1/2}$. Therefore, the expressions $\Delta_{|\pm 1\rangle}^{[100]}/P = a_1 \mp 2b$ or $\Delta_{|\pm 1\rangle}^{[110]}/P = a_1 + a_2 \pm (c - b)$ are also fully justified. To keep the formal-

ism in this work as consistent as possible with existing literature [43,46], we choose to work with the notation from Eq. (6).

So far, we considered the stress response of NV centers oriented as NV1 described by the tensor $\sigma_{XYZ} \equiv \sigma_{XYZ}^{\text{NV1}}$. To include the remaining three NV orientations, we express $\sigma_{XYZ}^{\text{NV1}}$ in the reference frames of NV2-4 by performing the coordinate system transformation

$$\sigma_{XYZ}^k = \mathbf{K}_k \cdot \sigma_{XYZ}^{\text{NV1}} \cdot \mathbf{K}_k^T \quad (7)$$

with $k \in \{\text{NV2}, \text{NV3}, \text{NV4}\}$. The rotations \mathbf{K}_k are given in Table I [for a definition of the rotation matrices $\mathbf{R}_n(\theta)$ see Appendix B]. We then replace σ_{IJ} in Eq. (3) with the corresponding values from σ_{XYZ}^k , thereby obtaining expressions for the coupling amplitudes of NV2-4. The stress-induced level shifts $\Delta_{|\pm 1\rangle}$ for NV2-4 are obtained as described and are summarized in Table II. Note that a *Mathematica* file is provided to reproduce our calculations in detail [50].

C. Spin-strain coupling expressed in NV coordinate systems xyz_k

Expressing the coupling between lattice deformation and NV spin in terms of stress (or strain, not shown) defined in XYZ leads to compact expressions for $\Delta_{|\pm 1\rangle}$ [see Eq. (6)]. Despite the simplicity of this approach, several past works employed a formalism based on strain defined in one of the NV coordinate systems xyz_k [18,28,42,45]. To unify the two notations and allow for comparison of published results, we now show in detail how the spin-stress description, with stress in XYZ , is translated into the strain framework, where strain is defined with respect to coordinate system xyz_k .

To find expressions for the spin-strain coupling amplitudes with the strain tensor defined in the reference frame of NV1, we follow the approach by Barson *et al.* [43] and link the stress tensor $\sigma_{XYZ}^{\text{NV1}}$ to the strain tensor $\epsilon_{xyz}^{\text{NV1}}$ via the elastic stiffness tensor $\tilde{\mathbf{C}}_{XYZ}$ by

$$\tilde{\sigma}_{XYZ}^{\text{NV1}} = \tilde{\mathbf{C}}_{XYZ} \tilde{\mathbf{L}}_{\text{NV1}}^T \tilde{\epsilon}_{xyz}^{\text{NV1}}. \quad (8)$$

Here, $\tilde{\mathbf{L}}_{\text{NV1}} = \tilde{\mathbf{R}}_{[001]}(-3\pi/4)\tilde{\mathbf{R}}_{[110]}(-\alpha_{\text{NV}})$ describes the coordinate system transformation from XYZ to xyz_{NV1} (see Table I and Appendix B for definition of rotation matrices). As indicated by $\tilde{\mathbf{L}}$ and $\tilde{\mathbf{R}}$, we express the transformation matrices \mathbf{L} and \mathbf{R} in Kelvin notation to write Hooke's law in vectorial form, where $\tilde{\sigma}$ and $\tilde{\epsilon}$ are 6×1 vectors and the stiffness tensor $\tilde{\mathbf{C}}$ is a 6×6 matrix (see Appendix A) [51,52]. We then replace σ_{IJ} in Eq. (3) with the result from Eq. (8) and obtain the NV1 spin-strain coupling amplitudes

$$M_x^{\text{NV1}} = B(\epsilon_{xx} - \epsilon_{yy}) + 2C\epsilon_{yz}, \quad (9a)$$

$$M_y^{\text{NV1}} = -2B\epsilon_{xy} - 2C\epsilon_{xz}, \quad (9b)$$

$$M_z^{\text{NV1}} = A_1\epsilon_{zz} + A_2(\epsilon_{xx} + \epsilon_{yy}), \quad (9c)$$

$$N_x^{\text{NV1}} = D(\epsilon_{xx} - \epsilon_{yy}) + 2E\epsilon_{yz}, \quad (9d)$$

$$N_y^{\text{NV1}} = -2D\epsilon_{xy} - 2E\epsilon_{xz}, \quad (9e)$$

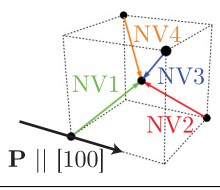
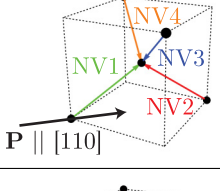
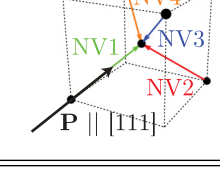
which depend on the spin-strain coupling constants

$$A_1 = a_1(C_{11} + 2C_{12}) + 4a_2C_{44}, \quad (10a)$$

$$A_2 = a_1(C_{11} + 2C_{12}) - 2a_2C_{44}, \quad (10b)$$

$$B = -b(C_{11} - C_{12}) - 2cC_{44}, \quad (10c)$$

TABLE II. Overview over NV orientations NV1-4 and the corresponding level shifts $\Delta_{|\pm 1\rangle}$ for $\mathbf{B} = 0$ and stresses along the [100], [110], and [111] directions, expressed in terms of stress (third column) and strain (fourth column). a_1 , a_2 , b , and c denote the spin-stress coupling constants while A_1 , A_2 , B , and C represent the spin-strain coupling constants. We use $\gamma = (C_{11} + 2C_{12})/C_{44}$, the Poisson ratio $\nu = C_{12}/(C_{11} + C_{12})$, and strain amplitude $\epsilon = P/E$, with $E = (C_{11} - C_{12})(C_{11} + 2C_{12})/(C_{11} + C_{12})$ being the Young's modulus, to shorten the expressions for strain-induced level shifts. Also note that the strain-induced level shifts are expressed in the engineering strain framework. To convert to pure strain, use $\gamma = 2(C_{11} + 2C_{12})/C_{44}$ (see Appendix D). (C_{11} , C_{12} , C_{44}) = (1076, 125, 576) GPa are the stiffness tensor components of diamond [48,49].

stress \mathbf{P}	NV orientation	$\Delta_{ \pm 1\rangle}/P$	$\Delta_{ \pm 1\rangle}/\epsilon$
 $\mathbf{P} \parallel [100]$	NV1	$a_1 \pm 2b$	$\frac{(1-2\nu)}{3}(A_1 + 2A_2) \pm \frac{(2+2\nu)}{3}(B - \sqrt{2}C)$
	NV2		
	NV3		
	NV4		
 $\mathbf{P} \parallel [110]$	NV1	$a_1 + a_2 \pm (b - c)$	$\pm \frac{1}{3} \left[B(\gamma(1-2\nu) - (1+\nu)) + \frac{C}{\sqrt{2}}(\gamma(1-2\nu) + 2(1+\nu)) \right]$
	NV2	$a_1 - a_2 \pm (b + c)$	$\pm \frac{1}{3} \left[B(\gamma(1-2\nu) + (1+\nu)) + \frac{C}{\sqrt{2}}(\gamma(1-2\nu) - 2(1+\nu)) \right]$
	NV3		
	NV4		
 $\mathbf{P} \parallel [111]$	NV1	$a_1 + 2a_2$	$\frac{1-2\nu}{3}((A_1 - A_2)\gamma + A_1 + 2A_2)$
	NV2	$a_1 - \frac{2}{3}a_2 \pm \frac{4}{3}c$	$\frac{1-2\nu}{9}(-(A_1 - A_2)\gamma + 3(A_1 + 2A_2))$
	NV3		$\pm \frac{2\sqrt{2}}{9}\gamma(1-2\nu)(C + \sqrt{2}B)$
	NV4		

$$C = \sqrt{2}b(C_{11} - C_{12}) - \sqrt{2}cC_{44}, \quad (10d)$$

$$D = -d(C_{11} - C_{12}) - 2eC_{44}, \quad (10e)$$

$$E = \sqrt{2}d(C_{11} - C_{12}) - \sqrt{2}eC_{44}. \quad (10f)$$

As our formalism relies on the engineering strain convention, the relations in Eq. (10) differ by a factor of 2 in the C_{44} terms compared to other work [43,53], where the pure strain convention is used (see Appendix D).

As is evident from Eq. (8), the form of the spin-strain coupling amplitudes in Eq. (9) for a given NV orientation depends on the rotation of the employed NV reference frame in the plane orthogonal to the NV quantization axis in strong contrast to the spin-stress coupling amplitudes from Eq. (3). For example, if one defines xyz such that the x axis lies in a symmetry plane, Eq. (9) becomes (see Appendix C)

$$M'_x = -B(\epsilon'_{xx} - \epsilon'_{yy}) + 2C\epsilon'_{xz}, \quad (11a)$$

$$M'_y = 2B\epsilon'_{xy} + 2C\epsilon'_{yz}, \quad (11b)$$

$$M'_z = A_1\epsilon'_{zz} + A_2(\epsilon'_{xx} + \epsilon'_{yy}), \quad (11c)$$

$$N'_x = -D(\epsilon'_{xx} - \epsilon'_{yy}) + 2E\epsilon'_{xz}, \quad (11d)$$

$$N'_y = 2D\epsilon'_{xy} + 2E\epsilon'_{yz}. \quad (11e)$$

Both definitions of xyz are valid, but care has to be taken since usually $\epsilon_{xyz} \neq \epsilon'_{xyz}$. To avoid possible confusion it is therefore generally advisable to describe strain or stress in an external reference frame, where the coupling amplitudes only depend on the direction of the NV quantization axis—a typical choice is the crystal coordinate system XYZ (see Appendix C).

For uniaxial stresses along the [100], [110], and [111] directions, the strain tensors in the NV1 reference frame obtained from Eq. (8) are

$$\epsilon_{xyz}^{[100]} = \epsilon \begin{pmatrix} \frac{1-\nu}{2} & \frac{1+\nu}{\sqrt{12}} & -\frac{1+\nu}{\sqrt{6}} \\ \frac{1+\nu}{\sqrt{12}} & \frac{1-5\nu}{6} & -\frac{1+\nu}{\sqrt{18}} \\ -\frac{1+\nu}{\sqrt{6}} & -\frac{1+\nu}{\sqrt{18}} & \frac{1-2\nu}{3} \end{pmatrix}, \quad (12a)$$

$$\epsilon_{xyz}^{[110]} = \epsilon \begin{pmatrix} \frac{2-2\nu-\gamma(1-2\nu)}{4} & 0 & 0 \\ 0 & \frac{2-10\nu+\gamma(1-2\nu)}{12} & \frac{-2-2\nu-\gamma(1-2\nu)}{72} \\ 0 & \frac{-2-2\nu-\gamma(1-2\nu)}{72} & \frac{2(1-2\nu)+\gamma(1-2\nu)}{6} \end{pmatrix}, \quad (12b)$$

$$\epsilon_{xyz}^{[111]} = \epsilon \begin{pmatrix} \frac{2(1-2\nu)-\gamma(1-2\nu)}{6} & 0 & 0 \\ 0 & \frac{2(1-2\nu)-\gamma(1-2\nu)}{6} & 0 \\ 0 & 0 & \frac{1-2\nu+\gamma(1-2\nu)}{3} \end{pmatrix}, \quad (12c)$$

where we introduced $\gamma = (C_{11} + 2C_{12})/C_{44}$, the Poisson ratio $\nu = C_{12}/(C_{11} + C_{12})$, and the strain amplitude $\epsilon = P/E$ to shorten the notation. P is the applied stress and $E = (C_{11} - C_{12})(C_{11} + 2C_{12})/(C_{11} + C_{12})$ is the Young's modulus [49]. The associated level shifts for $B = 0$, which we obtain by combining Eqs. (4), (9), and (12), are

$$\Delta_{|\pm 1\rangle}^{[100]}/\epsilon = \frac{(1-2\nu)}{3}(A_1 + 2A_2) \pm \frac{(2+2\nu)}{3}(B - \sqrt{2}C), \quad (13a)$$

$$\Delta_{|\pm 1\rangle}^{[110]}/\epsilon = \frac{1-2\nu}{6}[A_1(2+\gamma) - A_2(\gamma-4)] \pm \frac{1}{3}\{B[\gamma(1-2\nu) - (1+\nu)] + \frac{C}{\sqrt{2}}[\gamma(1-2\nu) + 2(1+\nu)]\}, \quad (13b)$$

$$\Delta_{|\pm 1\rangle}^{[111]}/\epsilon = \frac{1-2\nu}{3}[(A_1 - A_2)\gamma + A_1 + 2A_2]. \quad (13c)$$

To find the strain-induced level shifts for all four NV orientations, we follow a similar approach as before. We first use the relation

$$\tilde{\epsilon}_{xyz}^k = \tilde{L}_k \tilde{C}_{XYZ}^{-1} \tilde{\sigma}_{XYZ}^{NV1} \quad (14)$$

with the rotations \tilde{L}_k from Table I to express stress, defined in XYZ , in terms of strain defined in the reference frames of NV2-4. By replacing the strain tensor components ϵ_{ij}^{NV1} in Eq. (9) with the ϵ_{ij}^k from Eq. (14), we then obtain the spin-strain coupling amplitudes for NV2-4. The resulting level shifts are summarized in Table II.

Obviously, the expressions for the stress-induced level shifts, with stress defined in the crystal coordinate system XYZ , are much more compact. This observation, together with the fact that coupling amplitudes in XYZ only depend on the z direction of the employed NV reference frame, supports the notion that the formal description of spin-mechanical interaction is simplest when crystal deformation is defined in an external reference frame, for example the crystal coordinate system XYZ . Before we continue, we also want to point out that the presented formalism not only applies to the $S = 1$ ground-state manifold of the NV center, but can also be used to describe the influence of crystal deformation on the NV's $S = 1$ excited state [45] and the NV's $S = 0$ ground-state levels [33], where the orbital symmetries of the involved states are identical.

III. STRESS AND STRAIN IN CANTILEVERS

To illustrate how the coupling formalism developed here can be applied, we will now derive an expression for the stress tensor in singly clamped cantilever beams that are bent by a static external force \mathbf{V} . Such beams are currently the most common choice if spin-stress coupling in diamond-based hybrid spin-oscillator systems is to be quantified [18,28,43], since the occurring stress can be described analytically using a relatively simple approach.

A. Cantilever coordinate system $\tilde{x}\tilde{y}\tilde{z}$ and sign conventions

We begin our discussion by defining sign conventions for shear force, bending moment, coordinate directions, beam deflection, lateral forces, and strain or stress [54]. In general we consider a cantilever of length l , which has a rectangular cross section of width w and thickness t with $l \gg w, t$. The cantilever coordinate system $\tilde{x}\tilde{y}\tilde{z}$ is chosen such that length l is defined along $\mathbf{e}_{\tilde{x}}$, width w along $\mathbf{e}_{\tilde{y}}$, and thickness t along $\mathbf{e}_{\tilde{z}}$ [see Fig. 1(a)]. The \tilde{x} axis has its origin at the clamped end of the beam and \tilde{y} and \tilde{z} are defined with respect to the cross section's centroid. Points that lie within the beam

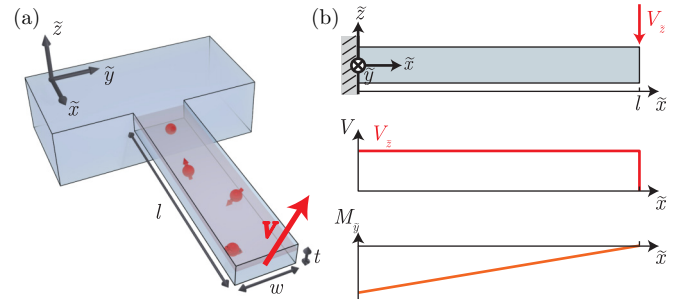


FIG. 1. Beam bending with a transverse force. (a) A singly clamped cantilever with dimensions width w , length l , and thickness t is subject to an external shear force $\mathbf{V} = (V_{\tilde{x}}, V_{\tilde{y}}, V_{\tilde{z}})^T$, which is applied at the tip of the cantilever, i.e., at $\tilde{x} = l$. (b) A positive shear force of amplitude $V_{\tilde{z}}$ pushes the cantilever downwards and induces a negative bending moment $M_{\tilde{y}}$. As the induced shear force remains constant along the beam, the bending moment decreases linearly from tip to root.

are therefore described by $\tilde{x} \in [0, l]$, $\tilde{y} \in [-w/2, w/2]$ and $\tilde{z} \in [-t/2, t/2]$. Lateral deflection u is chosen to be positive along $-\mathbf{e}_{\tilde{z}}$. Shear forces \mathbf{V} are defined positive if they cause the beam to rotate clockwise. For example, an external force pointing along $-\mathbf{e}_{\tilde{z}}$ and applied at positive \tilde{x} would rotate the beam clockwise about the \tilde{y} axis when looking along $\mathbf{e}_{\tilde{y}}$ and is therefore considered positive. Induced bending moments are defined to be positive if they correspond to a sagging behavior of the beam, while negative bending moments refer to hogging [scenario in Fig. 1(b)]. Finally, tension (compression) relates to positive (negative) strain and stress amplitudes.

B. Stress tensor of a singly clamped cantilever

To derive the stress tensor in a singly clamped cantilever, we consider a transverse force of magnitude $V_{\tilde{z}}$ that is applied at the tip of the beam and pushes it in the $-\mathbf{e}_{\tilde{z}}$ direction. This force induces the negative bending moment

$$M_{\tilde{y}}(\tilde{x}) = -(l - \tilde{x})V_{\tilde{z}} \quad (15)$$

for $\tilde{x} \in [0, l]$ and causes normal stress that points along $\mathbf{e}_{\tilde{x}}$. For a true beam, which satisfies $l \gg w, t$, we can apply the flexural formula [54–56] to find the induced normal stress

$$\sigma_n(\tilde{x}, \tilde{z}) = -\frac{\tilde{z}}{I_{\tilde{z}}} M_{\tilde{y}}(\tilde{x}) = \frac{\tilde{z}(l - \tilde{x})}{I_{\tilde{z}}} V_{\tilde{z}} \quad (16)$$

with the moment of inertia $I_{\tilde{z}} = wt^3/12$. Bending the cantilever downwards induces tensile stress in the top half of the beam ($\tilde{z} > 0$) and compressive stress in the lower half ($\tilde{z} < 0$). Moreover, $\sigma_n(\tilde{x}, \tilde{z})$ decreases linearly from root to tip and from the neutral plane, i.e., the plane with $\tilde{z} = 0$, towards top and bottom surfaces at $\tilde{z} = \pm t/2$. In addition to normal stress, the applied transverse force also gives rise to shear stress

$$\sigma_s(\tilde{z}) = \frac{V_{\tilde{z}}}{2I_{\tilde{z}}} \left[\left(\frac{t}{2} \right)^2 - \tilde{z}^2 \right] \quad (17)$$

in the cantilever [54], which vanishes at the top and bottom surfaces and is maximized in the beam's neutral plane.

To link this discussion to the spin-stress coupling amplitudes in the previous section [see, e.g., Eq. (3)], we now

formulate a stress tensor that corresponds to the influence of an external shear force $\mathbf{V} = (V_{\tilde{x}}, V_{\tilde{y}}, V_{\tilde{z}})^T$ applied to a cantilever as shown in Fig. 1(a). In our example, the cantilever is oriented such that its coordinate system $\tilde{x}\tilde{y}\tilde{z}$ coincides with the crystal coordinate system XYZ . The axial force component $V_{\tilde{x}}$ causes a constant normal stress $\sigma_{XX} = V_{\tilde{x}}/A$ along the beam where $A = wt$ is the beam's cross-sectional area. As

$$\sigma_{XYZ}^c = \begin{pmatrix} \frac{V_{\tilde{x}}}{wt} + (l - \tilde{x})\left(\frac{\tilde{z}V_{\tilde{z}}}{I_z} + \frac{\tilde{y}V_{\tilde{y}}}{I_y}\right) & \frac{V_{\tilde{y}}}{2I_y}\left[\left(\frac{w}{2}\right)^2 - \tilde{y}^2\right] & \frac{V_{\tilde{z}}}{2I_z}\left[\left(\frac{t}{2}\right)^2 - \tilde{z}^2\right] \\ \frac{V_{\tilde{y}}}{2I_y}\left[\left(\frac{w}{2}\right)^2 - \tilde{y}^2\right] & 0 & 0 \\ \frac{V_{\tilde{z}}}{2I_z}\left[\left(\frac{t}{2}\right)^2 - \tilde{z}^2\right] & 0 & 0 \end{pmatrix}. \quad (18)$$

Under the assumption of a purely transverse force along $-\mathbf{e}_{\tilde{z}}$, the stress tensor close to the beam's top surface simplifies to

$$\sigma_{XYZ}^c = P(\tilde{x}, \tilde{z}) \begin{pmatrix} 1 & 0 & 0 \\ 0 & 0 & 0 \\ 0 & 0 & 0 \end{pmatrix} \quad (19)$$

with $P(\tilde{x}, \tilde{z}) = \frac{\tilde{z}V_{\tilde{z}}}{I_z}(l - \tilde{x})$ being the applied stress amplitude. We point out that pushing along $-\mathbf{e}_{\tilde{z}}$ on a cantilever oriented along the [100] direction introduces uniaxial stress along the [100] direction. Consequently, stress in cantilevers of different orientations can be obtained by making an appropriate coordinate system transformation.

From an experimental point of view, it is often desirable to express $P(\tilde{x}, \tilde{z})$ in terms of the induced cantilever deflection u . From Euler-Bernoulli beam theory we know that a force $V_{\tilde{z}}$ applied at the beam's end causes a beam deflection $u(\tilde{x})$ of the form [56]

$$u(\tilde{x}) = \frac{V_{\tilde{z}}}{EI_{\tilde{z}}} \left(\frac{l\tilde{x}^2}{2} - \frac{\tilde{x}^3}{6} \right). \quad (20)$$

We can thus link the applied force $V_{\tilde{z}}$ to the maximum beam displacement $u(l)$ via the expression

$$V_{\tilde{z}} = \frac{3EI_{\tilde{z}}}{l^3}u(l), \quad (21)$$

and the stress amplitude $P(\tilde{x}, \tilde{z})$ becomes

$$P(\tilde{x}, \tilde{z}) = \frac{3\tilde{z}E}{l^3}(l - \tilde{x})u(l), \quad (22)$$

where $u(l)$ now represents the cantilever deflection measured at $\tilde{x} = l$ and E is the Young's modulus.

IV. DETERMINING SPIN-STRESS COUPLING CONSTANTS IN DIAMOND-BASED HYBRID SYSTEMS

After establishing a full and consistent treatment of spin-stress coupling in the NV ground state and deriving an expression for the stress tensor in a singly clamped cantilever, we now present bending experiments which we performed to characterize the spin-stress and spin-strain coupling constants. In our original analysis of these measurements by Teissier *et al.* [28], we used an oversimplified theoretical description

we know from Eqs. (16) and (17), the transverse component $V_{\tilde{z}} \parallel -\mathbf{e}_{\tilde{z}}$ induces normal stress $\sigma_{XX} = V_{\tilde{z}}\tilde{z}(l - \tilde{x})/I_z$ as well as shear stresses $\sigma_{XZ} = \sigma_{ZX} = V_{\tilde{z}}[(t/2)^2 - \tilde{z}^2]/2I_z$. In analogy, the transverse component $V_{\tilde{y}} \parallel +\mathbf{e}_{\tilde{y}}$ causes normal stress $\sigma_{YY} = V_{\tilde{y}}\tilde{y}(l - \tilde{x})/I_y$ and shear stresses $\sigma_{XY} = \sigma_{YX} = V_{\tilde{y}}[(w/2)^2 - \tilde{y}^2]/2I_y$ with $I_y = tw^3/12$. All in all, the final stress tensor for small cantilever deflections is

of the coupling mechanism, which neglected shear strain and the Poisson effect. With the formalism developed here, we can now extract the correct spin-stress coupling constants and compare them to existing literature.

The diamond cantilevers investigated by Teissier *et al.* were aligned such that $\mathbf{e}_{\tilde{x}} \parallel [110]$ and $\mathbf{e}_{\tilde{z}} \parallel [001]$, had dimensions of $(w \times l \times t) = (3.5 \times 10 - 50 \times 0.2 - 1) \mu\text{m}^3$ and contained shallow implanted NV centers, which were located $\sim 17 \text{ nm}$ below the top surface. We used a metal tip, placed at $\tilde{x} = l$, to displace the cantilever along $\mathbf{e}_{\tilde{z}}$. The resulting stress tensor reads

$$\sigma_{XYZ}^{[110]} = \frac{P}{2} \begin{pmatrix} 1 & 1 & 0 \\ 1 & 1 & 0 \\ 0 & 0 & 0 \end{pmatrix}, \quad (23)$$

where the stress amplitude for shallow NV centers ($\tilde{z} \approx t/2$) located at the cantilever's base ($\tilde{x} \approx 0$) is given by [see Eq. (22)]

$$P \equiv P(0, t/2) = \frac{3}{2} \frac{t}{l^2} Eu. \quad (24)$$

Since the metallic tip (tungsten) was about three orders of magnitude stiffer than the cantilever, the beam deflection u was directly given by the piezo displacement amplitude of the tip.

For stress along the [110] direction, the four possible NV orientations can be grouped into two subgroups with respect to their stress-induced level shifts and splittings: NV1+2 and NV3+4, which we will refer to as NVA and NVB in the following. The associated level shifts are (see Table II)

$$\Delta_{|\pm 1\rangle}^{\text{NVA}}/P = (a_1 + a_2) \pm (b - c), \quad (25a)$$

$$\Delta_{|\pm 1\rangle}^{\text{NVB}}/P = (a_1 - a_2) \pm (b + c). \quad (25b)$$

To unambiguously identify all four spin-stress coupling constants, we investigated the stress-induced level shifts for both NV orientations by performing optically detected electron-spin-resonance (ESR) measurements (see Appendix E for the analyzed ESR data sets) [28]. We then

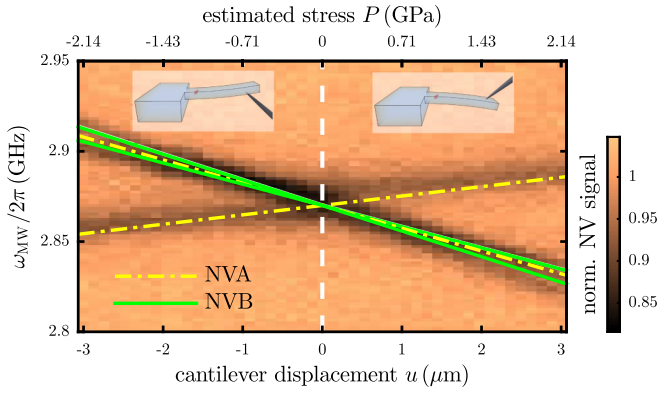


FIG. 2. Comparing experimental data with expected stress-induced level shifts (yellow dashed-dotted lines denote predictions for NV family NVA and green solid lines represent NV orientation NVB) yields a very good agreement between predicted spin-stress coupling parameters and our experiment.

extracted spin sublevel shifts $\Delta_{\parallel}^{\text{NVA},\text{NVB}}$ and splittings $\Delta_{\perp}^{\text{NVA},\text{NVB}}$ as

$$\Delta_{\parallel}^{\text{NVA}} P \equiv (\Delta_{|+1\rangle}^{\text{NVA}} + \Delta_{|-1\rangle}^{\text{NVA}})/2 = (a_1 + a_2)P, \quad (26a)$$

$$\Delta_{\perp}^{\text{NVA}} P \equiv (\Delta_{|+1\rangle}^{\text{NVA}} - \Delta_{|-1\rangle}^{\text{NVA}})/2 = (b - c)P, \quad (26b)$$

$$\Delta_{\parallel}^{\text{NVB}} P \equiv (\Delta_{|+1\rangle}^{\text{NVB}} + \Delta_{|-1\rangle}^{\text{NVB}})/2 = (a_1 - a_2)P, \quad (26c)$$

$$\Delta_{\perp}^{\text{NVB}} P \equiv (\Delta_{|+1\rangle}^{\text{NVB}} - \Delta_{|-1\rangle}^{\text{NVB}})/2 = (b + c)P. \quad (26d)$$

Finally, the spin-stress coupling constants are given by

$$a_1 = (\Delta_{\parallel}^{\text{NVA}} + \Delta_{\parallel}^{\text{NVB}})/2, \quad (27a)$$

$$a_2 = (\Delta_{\parallel}^{\text{NVA}} - \Delta_{\parallel}^{\text{NVB}})/2, \quad (27b)$$

$$b = (\Delta_{\perp}^{\text{NVA}} + \Delta_{\perp}^{\text{NVB}})/2, \quad (27c)$$

$$c = (\Delta_{\perp}^{\text{NVB}} - \Delta_{\perp}^{\text{NVA}})/2. \quad (27d)$$

We measured $\Delta_{\parallel}^{\text{NVA},\text{NVB}}$ and $\Delta_{\perp}^{\text{NVA},\text{NVB}}$ for a total of five NV centers (three from orientation NVA and two from NVB; see Appendix E) and determined the values

$$a_1 = (-11.7 \pm 3.2)\text{MHz/GPa}, \quad (28a)$$

$$a_2 = (6.5 \pm 3.2)\text{MHz/GPa}, \quad (28b)$$

$$b = (7.1 \pm 0.8)\text{MHz/GPa}, \quad (28c)$$

$$c = (-5.4 \pm 0.8)\text{MHz/GPa} \quad (28d)$$

for the spin-stress coupling constants. The given errors denote 68% confidence intervals. They are rather large as the small number of NV centers we analyzed in our experiments was not sufficient to deal with systematic errors induced by, e.g., different environmental stress fields resulting from crystal defects, surface roughness, or the proximity of cantilever edges. Despite the large uncertainties, we find a very good agreement between the theoretically expected level shifts based on the spin-stress coupling constants in Eq. (28) and typical experimental data shown in Fig. 2. Finally, the spin-strain coupling

TABLE III. Comparing spin-stress coupling constants from [28] and [43]. The two sets of values differ by a factor of $\sim 2-3$ as well as in their signs, which can be explained by a potentially imprecise determination of cantilever dimensions in [28] and different sign conventions for tensile/compressive stress.

	This work MHz/GPa	Barson <i>et al.</i> [43] MHz/GPa
a_1	-11.7 ± 3.2	4.86 ± 0.02
a_2	6.5 ± 3.2	-3.7 ± 0.2
b	7.1 ± 0.8	-2.3 ± 0.3
c	-5.4 ± 0.8	3.5 ± 0.3

constants A_1, A_2, B, C

$$A_1 = (-0.5 \pm 8.6)\text{GHz/strain}, \quad (29a)$$

$$A_2 = (-9.2 \pm 5.7)\text{GHz/strain}, \quad (29b)$$

$$B = (-0.5 \pm 1.2)\text{GHz/strain}, \quad (29c)$$

$$C = (14.0 \pm 1.3)\text{GHz/strain} \quad (29d)$$

are obtained via Eq. (10).

Similar values for the stress coupling constants, obtained through applying uniaxial stress to a diamond cube in a diamond-anvil cell, were reported recently [43]. Comparing the two sets of values (see Table III) shows that both experiments find spin-stress coupling constants on the order of a few MHz/GPa, yet they differ by a factor $\sim 2-3$ and in their signs. The origin of the sign discrepancy lies in different sign conventions for the applied stress. In Barson *et al.* [43], compressive stress is defined to have positive amplitudes and causes the NV zero-field splitting D_0 to increase. In our analysis, however, compressive stress is negative and increases D_0 (see Fig. 2). Consequently, the spin-stress coupling constants have different signs. We tentatively assign the mismatch in amplitude to uncertainties in the cantilever dimensions, caused by imperfections in diamond fabrication. Note that uncertainties in l pose a serious problem as the applied stress amplitude P is proportional to l^{-2} . A potential measurement error in l of 25% would result in values for stress coupling parameters almost identical in amplitude to the values reported by Barson *et al.* [43]. We thus suggest similar experiments to be conducted on better-defined geometries to reduce the uncertainty in cantilever dimensions.

V. SUMMARY AND OUTLOOK

To summarize, we give a complete description of how the coupling between lattice deformation and the spin degree of freedom of all four possible NV orientations can be described in terms of stress or strain, defined in crystal coordinates XYZ or individual NV reference frames. We show that the formal treatment of spin-mechanical interaction is simplest and most compact when strain or stress are described within XYZ . We therefore advocate the adoption of this approach for future advances in the field. We further illustrate how the presented formalism can be used to determine the spin-stress and spin-strain coupling constants. To that end, we derive

the stress tensor in a singly clamped cantilever and use it to reanalyze measurements from Teissier *et al.* [28]. We find that the extracted values for the spin-stress coupling constants are in good agreement with other values reported in the literature, but also point out differences in employed sign conventions.

With a correct and consistent framework at hand, we can now complete the characterization of spin-stress coupling in the NV $S = 1$ ground state by quantifying the remaining spin-stress coupling constants d and e [46]. In our presented experiments, this was not possible as the relevant coupling $H_{\sigma 1}$ between $|0\rangle$ and the $|\pm 1\rangle$ manifold was far off resonance. Experiments appropriate for this task could be based on static or low-frequency stress fields and would require external magnetic fields of $B_z \approx 1025$ G to study spin-stress coupling at the ground-state level anticrossing (GSLAC), where the relevant spin sublevels are close in energy. Coupling constants d and e could then for example be determined via dressed state spectroscopy [39] or the observation of stress-induced Rabi oscillations [46].

ACKNOWLEDGMENTS

We thank M. Barson, M. Doherty, and A. Pályi for fruitful discussions. We gratefully acknowledge financial support through the NCCR QSIT, a competence center funded by the Swiss NSF and through the Swiss Nanoscience Institute (SNI).

APPENDIX A: KELVIN NOTATION

For small strains or stresses, Hooke's law describes the linear stress-strain relationship,

$$\sigma_{IJ} = \sum_{KL} C_{IJKL} \epsilon_{KL}, \quad (\text{A1})$$

where C_{IJKL} are the components of the elastic stiffness tensor, which is a fourth rank tensor and in principle contains $3 \times 3 \times 3 = 81$ independent elements. However, as stress and strain tensors are symmetric, this number is reduced to 36. For cubic crystals, such as diamond, symmetry arguments further reduce the number of independent elements to 3 [49].

To write Hooke's law in vectorial form, we employ the Kelvin notation in which (A1) becomes

$$\tilde{\sigma}_{XYZ} = \tilde{C}_{XYZ} \tilde{\epsilon}_{XYZ}. \quad (\text{A2})$$

$$\tilde{N} = \begin{pmatrix} 0 & 0 & 0 & 0 & \sqrt{2}n_2 & -\sqrt{2}n_3 \\ 0 & 0 & 0 & -\sqrt{2}n_1 & 0 & \sqrt{2}n_3 \\ 0 & 0 & 0 & \sqrt{2}n_1 & -\sqrt{2}n_2 & 0 \\ 0 & \sqrt{2}n_1 & -\sqrt{2}n_1 & 0 & n_3 & -p_2 \\ -\sqrt{2}n_2 & 0 & \sqrt{2}n_2 & -n_3 & 0 & n_1 \\ \sqrt{2}n_3 & -\sqrt{2}n_3 & 0 & n_2 & -n_1 & 0 \end{pmatrix}. \quad (\text{B4})$$

APPENDIX C: HOW THE DEFINITION OF xyz INFLUENCES SPIN-STRAIN COUPLING AMPLITUDES

To clarify the influence of NV reference frame definitions for a given NV quantization axis on the presented formalism,

Here, the elastic stiffness tensor reduces to a 6×6 tensor,

$$\tilde{C}_{XYZ} = \begin{pmatrix} C_{11} & C_{12} & C_{12} & 0 & 0 & 0 \\ C_{12} & C_{11} & C_{12} & 0 & 0 & 0 \\ C_{12} & C_{12} & C_{11} & 0 & 0 & 0 \\ 0 & 0 & 0 & 2C_{44} & 0 & 0 \\ 0 & 0 & 0 & 0 & 2C_{44} & 0 \\ 0 & 0 & 0 & 0 & 0 & 2C_{44} \end{pmatrix}, \quad (\text{A3})$$

which contains only three independent elements $\{C_{11}, C_{12}, C_{44}\} = \{1076, 125, 576\}$ GPa for the diamond lattice symmetry [48,49,56,57]. Strain and stress tensors are written as the vectors

$$\tilde{\epsilon}_{XYZ} = (\epsilon_{XX}, \epsilon_{YY}, \epsilon_{ZZ}, \sqrt{2}\epsilon_{YZ}, \sqrt{2}\epsilon_{XZ}, \sqrt{2}\epsilon_{XY})^T \quad (\text{A4})$$

and

$$\tilde{\sigma}_{XYZ} = (\sigma_{XX}, \sigma_{YY}, \sigma_{ZZ}, \sqrt{2}\sigma_{YZ}, \sqrt{2}\sigma_{XZ}, \sqrt{2}\sigma_{XY})^T. \quad (\text{A5})$$

APPENDIX B: DEFINITION OF ROTATION MATRICES

The rotation matrices $\mathbf{R}_n(\theta)$ from Table I describe three-dimensional rotations by angles θ about axes indicated by the unit vectors $\mathbf{n} = (n_1, n_2, n_3)^T$. $\mathbf{R}_n(\theta)$ is calculated using the relation [51]

$$\mathbf{R}_n(\theta) = \mathbb{1} + \sin \theta \mathbf{N} + (1 - \cos \theta) \mathbf{N}^2 \quad (\text{B1})$$

with

$$\mathbf{N} = \begin{pmatrix} 0 & -n_3 & n_2 \\ n_3 & 0 & -n_1 \\ -n_2 & n_1 & 0 \end{pmatrix}. \quad (\text{B2})$$

In this work, the axis of rotation \mathbf{n} is generally defined with respect to the original, unrotated coordinate system, and θ is positive for a clockwise rotation observed along \mathbf{n} .

When working with the Kelvin notation, we employ the rotation matrices

$$\begin{aligned} \tilde{\mathbf{R}}_n(\theta) &= \tilde{\mathbb{1}} + \sin \theta \tilde{\mathbf{N}} + (1 - \cos \theta) \tilde{\mathbf{N}}^2 \\ &\quad + \frac{1}{3} \sin \theta (1 - \cos \theta) (\tilde{\mathbf{N}} + \tilde{\mathbf{N}}^3) \\ &\quad + \frac{1}{6} (1 - \cos \theta)^2 (\tilde{\mathbf{N}}^2 + \tilde{\mathbf{N}}^4) \end{aligned} \quad (\text{B3})$$

with $\mathbf{n} = (n_1, n_2, n_3)^T$ and [51]

we compare spin-strain coupling amplitudes obtained for different xyz by following the derivation in Udvarhelyi *et al.* [46]. In the reference frame $xyz^{(a)}$, defined by $\mathbf{e}_x^{(a)} \parallel [\bar{1}10]$, $\mathbf{e}_y^{(a)} \parallel [\bar{1}\bar{1}2]$, and $\mathbf{e}_z^{(a)} \parallel [111]$, the y axis lies in a mirror

plane of the NV center and we find the spin-strain coupling amplitudes [see Eq. (9)]

$$M_x^{(a)} = B(\epsilon_{xx}^{(a)} - \epsilon_{yy}^{(a)}) + 2C\epsilon_{yz}^{(a)}, \quad (\text{C1a})$$

$$M_y^{(a)} = -2B\epsilon_{xy}^{(a)} - 2C\epsilon_{xz}^{(a)}, \quad (\text{C1b})$$

$$M_z^{(a)} = A_1\epsilon_{zz}^{(a)} + A_2(\epsilon_{xx}^{(a)} + \epsilon_{yy}^{(a)}). \quad (\text{C1c})$$

Here, $\epsilon_{xyz}^{(a)}$ is the strain tensor that describes crystal deformation in the reference frame $xyz^{(a)}$, and we neglect N_x and N_y for simplicity. However, when defining a second $xyz^{(b)}$ coordinate

system with $\mathbf{e}_x^{(b)} \parallel [\bar{1}\bar{1}2]$, $\mathbf{e}_y^{(b)} \parallel [1\bar{1}0]$, and $\mathbf{e}_z^{(b)} \parallel [111]$, the x axis lies in a mirror plane of the NV and the spin-strain coupling amplitudes are [see Eq. (11)]

$$M_x^{(b)} = -B(\epsilon_{xx}^{(b)} - \epsilon_{yy}^{(b)}) + 2C\epsilon_{xz}^{(b)}, \quad (\text{C2a})$$

$$M_y^{(b)} = 2B\epsilon_{xy}^{(b)} + 2C\epsilon_{yz}^{(b)}, \quad (\text{C2b})$$

$$M_z^{(b)} = A_1\epsilon_{zz}^{(b)} + A_2(\epsilon_{xx}^{(b)} + \epsilon_{yy}^{(b)}). \quad (\text{C2c})$$

Since both NV reference frames in this example share the same quantization axis, we expect identical strain-induced level shifts, which are given by

$$\begin{aligned} \Delta_{|\pm 1\rangle}^{(a)}/\epsilon &= [A_1\epsilon_{zz}^{(a)} + A_2(\epsilon_{xx}^{(a)} + \epsilon_{yy}^{(a)})] \\ &\pm [B^2(\epsilon_{xx}^{(a)} - \epsilon_{yy}^{(a)})^2 + 4BC\epsilon_{yz}^{(a)}(\epsilon_{xx}^{(a)} - \epsilon_{yy}^{(a)}) + 4C^2\epsilon_{yz}^{(a)2} + 4B^2\epsilon_{xy}^{(a)2} + 8BC\epsilon_{xy}^{(a)}\epsilon_{xz}^{(a)} + 4C^2\epsilon_{xz}^{(a)2}]^{1/2}, \end{aligned} \quad (\text{C3})$$

$$\begin{aligned} \Delta_{|\pm 1\rangle}^{(b)}/\epsilon &= [A_1\epsilon_{zz}^{(b)} + A_2(\epsilon_{xx}^{(b)} + \epsilon_{yy}^{(b)})] \\ &\pm [B^2(\epsilon_{xx}^{(b)} - \epsilon_{yy}^{(b)})^2 - 4BC\epsilon_{xz}^{(b)}(\epsilon_{xx}^{(b)} - \epsilon_{yy}^{(b)}) + 4C^2\epsilon_{xz}^{(b)2} + 4B^2\epsilon_{xy}^{(b)2} + 8BC\epsilon_{xy}^{(b)}\epsilon_{yz}^{(b)} + 4C^2\epsilon_{yz}^{(b)2}]^{1/2}, \end{aligned} \quad (\text{C4})$$

where ϵ is the applied strain amplitude. However, $\Delta_{|\pm 1\rangle}^{(a)} = \Delta_{|\pm 1\rangle}^{(b)}$ is only true when acknowledging that $\epsilon_{xyz}^{(a)} \neq \epsilon_{xyz}^{(b)}$ [for the chosen NV reference frames $\tilde{\epsilon}_{xyz}^{(b)} = (\epsilon_{xx}^{(a)}, \epsilon_{yy}^{(a)}, \epsilon_{zz}^{(a)}, -\sqrt{2}\epsilon_{xz}^{(a)}, \sqrt{2}\epsilon_{yz}^{(a)}, -\sqrt{2}\epsilon_{xy}^{(a)})^T$]. A simple and effective way to avoid possible confusion is to express crystal deformation in a reference frame external to the NV center. A typical choice is the crystal coordinate system XYZ used in this work. By replacing the strain tensor components in Eqs. (C1) and (C2) with

$$\tilde{\epsilon}_{xyz}^{(a,b)} = \tilde{\mathbf{L}}^{(a,b)} \tilde{\mathbf{C}}_{XYZ}^{-1} \tilde{\boldsymbol{\sigma}}_{XYZ}, \quad (\text{C5})$$

where

$$\tilde{\mathbf{L}}^{(a)} = \tilde{\mathbf{R}}_{[001]}(-3\pi/4) \tilde{\mathbf{R}}_{[110]}(-\alpha_{NV}),$$

$$\tilde{\mathbf{L}}^{(b)} = \tilde{\mathbf{R}}_{[001]}(-5\pi/4) \tilde{\mathbf{R}}_{[110]}(-\alpha_{NV}),$$

we find the identical spin-stress coupling constants given in Eq. (3) of the main text. Note that these are identical for any xyz as long as the employed NV reference frame shares the same z axis. Describing crystal deformation in XYZ therefore simplifies the presented formalism significantly.

APPENDIX D: ENGINEERING VS PURE STRAIN

When using Hooke's law, confusion often arises due to the difference between pure and engineering strain notations. We briefly demonstrate here that using different strain conventions does not affect the general structure of the framework presented in this paper. However, small corrections to the relations used to convert spin-stress coupling constants into their spin-strain counterparts [see Eq. (10)], as well as to the strain-induced level shifts and splittings $\Delta_{|\pm 1\rangle}$ from Table II are required.

In matrix form, the strain tensor is written as

$$\epsilon_{XYZ} = \begin{pmatrix} \epsilon_{XX} & \epsilon_{XY} & \epsilon_{XZ} \\ \epsilon_{YX} & \epsilon_{YY} & \epsilon_{YZ} \\ \epsilon_{ZX} & \epsilon_{ZY} & \epsilon_{ZZ} \end{pmatrix}, \quad (\text{D1})$$

where ϵ_{IJ} refers to the pure strain tensor components. However, to ensure the conservation of elastic energy when employing Hooke's law, the engineering strain notation is employed. A good example is the Voigt notation, in which

$$\tilde{\epsilon}_{XYZ}^V = (\epsilon_{XX}, \epsilon_{YY}, \epsilon_{ZZ}, \gamma_{YZ}, \gamma_{XZ}, \gamma_{XY})^T \quad (\text{D2})$$

also depends on the engineering shear strain components $\gamma_{IJ} = 2\epsilon_{IJ}$, which are twice the pure shear strain components. However, in this work we employ the Kelvin notation, as the Voigt notation does not allow the application of standard vector operations, such as coordinate system transformations through vector rotations. In the Kelvin notation, engineering strain shows up as factors of 2 in front of the C_{44} stiffness tensor components [see Eq. (A3)]. The formalism we present in this paper is therefore based on engineering strain.

This is important to note, as other works [43,53] rely on a spin-strain coupling formalism based on pure strain, and consequently employ slightly different expressions for the conversion relations of spin-stress into spin-strain coupling constants [see Eq. (10)] and the strain-induced level shifts $\Delta_{|\pm 1\rangle}$ (see Table II). Based on the brief explanation above, we can convert our engineering strain expressions into the pure strain framework [43,53] by replacing $C_{44} \rightarrow C_{44}/2$ in Eq. (10). The conversion relations for spin-stress into spin-strain coupling constants become

$$A_1 = a_1(C_{11} + 2C_{12}) + 2a_2C_{44}, \quad (\text{D3a})$$

$$A_2 = a_1(C_{11} + 2C_{12}) - a_2C_{44}, \quad (\text{D3b})$$

$$B = -b(C_{11} - C_{12}) - cC_{44}, \quad (\text{D3c})$$

$$C = \sqrt{2}b(C_{11} - C_{12}) - 1/\sqrt{2}cC_{44}, \quad (\text{D3d})$$

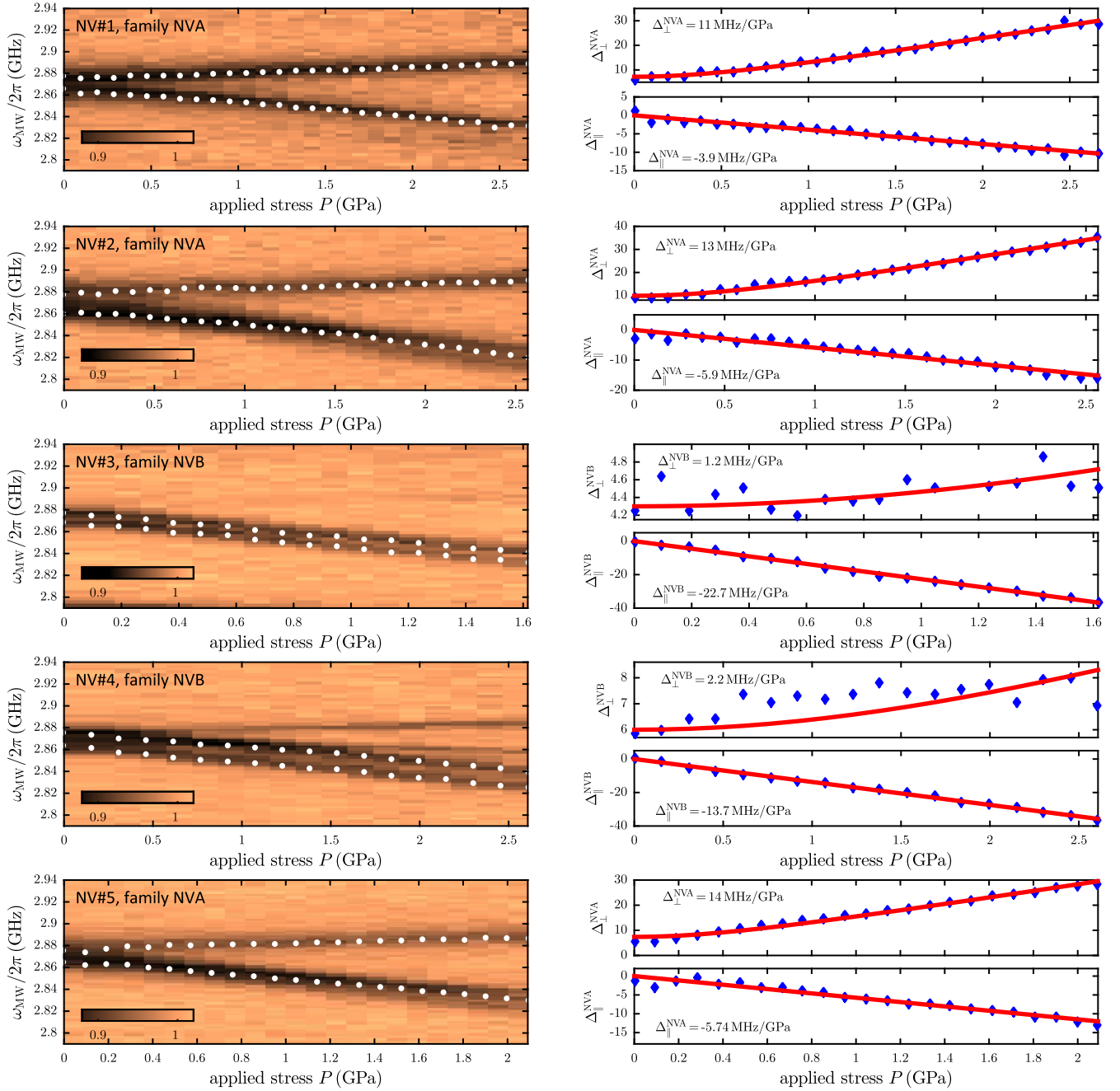


FIG. 3. Reactions of different NV centers to stress induced by cantilever bending. While the three NVs from family NVA show comparable shifts and splittings, the two NVs from family NVB react quite differently to stress, causing rather large uncertainties in the stress-coupling constants. Increasing statistics, i.e., by studying more NV centers and their response to stress, is required. White dotted lines in the left column represent ESR peak positions, determined by fits to our original data. In the right column, blue symbols denote experimentally obtained values for level shifts and splittings and red lines are fits to these to extract spin-stress coupling constants. $\Delta_{\parallel,\perp}^{A,B}$ are given in units of MHz. Note that our fits account for the presence of stress that was intrinsic to the sample.

$$D = -d(C_{11} - C_{12}) - eC_{44}, \quad (\text{D3e})$$

$$E = \sqrt{2}d(C_{11} - C_{12}) - 1/\sqrt{2}eC_{44}, \quad (\text{D3f})$$

$$B = (-3.7 \pm 0.9)\text{GHz/strain}, \quad (\text{D4c})$$

$$C = (11.8 \pm 1.1)\text{GHz/strain} \quad (\text{D4d})$$

and yield the values

$$A_1 = (-8.0 \pm 5.7)\text{GHz/strain}, \quad (\text{D4a})$$

$$A_2 = (-12.4 \pm 4.7)\text{GHz/strain}, \quad (\text{D4b})$$

for the spin-strain coupling constants. Clearly, these values differ significantly from those given in the main text [see Eq. (29a)]. Yet both strain conventions yield identical results for the strain-induced level shifts, if in the pure strain framework the $\Delta_{|\pm 1\rangle}$ contain the corrected $\gamma = 2(C_{11} + 2C_{12})/C_{44}$.

It is thus of utmost importance that the employed strain framework is well defined if spin-strain coupling constants are to be compared or even determined.

APPENDIX E: DETERMINATION OF SPIN-STRESS COUPLING CONSTANTS

As mentioned in the main text, we analyzed the stress-induced level shifts and splittings of five different NV centers.

Three of these were of orientation NVA and two belonged to NVB. Figure 3 shows the taken ESR data and the extracted values of level shifts Δ_{\parallel} and splittings Δ_{\perp} . White dots in the left column denote Lorentzian fits to determine the ESR dip positions. Blue dots in the right column represent calculated values for level shifts and splittings, while red lines are fits to extract level shifts and splittings per GPa of applied stress.

-
- [1] P. Treutlein, C. Genes, K. Hammerer, M. Poggio, and P. Rabl, in *Cavity Optomechanics*, Quantum Science and Technology, edited by M. Aspelmeyer, T. J. Kippenberg, and F. Marquardt (Springer, Berlin, Heidelberg, 2014), pp. 327–351.
 - [2] D. Lee, K. W. Lee, J. V. Cady, P. Ouartchaiyapong, and A. C. B. Jayich, *J. Opt.* **19**, 033001 (2017).
 - [3] M. D. LaHaye, J. Suh, P. M. Echternach, K. C. Schwab, and M. L. Roukes, *Nature (London)* **459**, 960 (2009).
 - [4] A. D. O’Connell, M. Hofheinz, M. Ansmann, R. C. Bialczak, M. Lenander, E. Lucero, M. Neeley, D. Sank, H. Wang, M. Weides, J. Wenner, J. M. Martinis, and A. N. Cleland, *Nature (London)* **464**, 697 (2010).
 - [5] J.-M. Pirkkalainen, S. U. Cho, J. Li, G. S. Paraoanu, P. J. Hakonen, and M. A. Sillanpää, *Nature (London)* **494**, 211 (2013).
 - [6] I. Martin, A. Shnirman, L. Tian, and P. Zoller, *Phys. Rev. B* **69**, 125339 (2004).
 - [7] D. Hunger, S. Camerer, T. W. Hänsch, D. König, J. P. Kotthaus, J. Reichel, and P. Treutlein, *Phys. Rev. Lett.* **104**, 143002 (2010).
 - [8] S. Camerer, M. Korppi, A. Jöckel, D. Hunger, T. W. Hänsch, and P. Treutlein, *Phys. Rev. Lett.* **107**, 223001 (2011).
 - [9] A. Jöckel, A. Faber, T. Kampschulte, M. Korppi, M. T. Rakher, and P. Treutlein, *Nat. Nanotechnol.* **10**, 55 (2015).
 - [10] D. Rugar, R. Budakian, H. J. Mamin, and B. W. Chui, *Nature (London)* **430**, 329 (2004).
 - [11] O. Arcizet, V. Jacques, A. Siria, P. Poncharal, P. Vincent, and S. Seidelin, *Nat. Phys.* **7**, 879 (2011).
 - [12] S. Kolkowitz, A. C. Bleszynski Jayich, Q. P. Unterreithmeier, S. D. Bennett, P. Rabl, J. G. E. Harris, and M. D. Lukin, *Science* **335**, 1603 (2012).
 - [13] K. Xia and J. Twamley, *Phys. Rev. B* **94**, 205118 (2016).
 - [14] I. Yeo, P.-L. de Assis, A. Gloppe, E. Dupont-Ferrier, P. Verlot, N. Malik, E. Dupuy, J. Claudon, J.-M. Gerard, A. Auffeves, G. Nogues, S. Seidelin, J.-P. Poizat, O. Arcizet, and M. Richard, *Nat. Nanotechnol.* **9**, 106 (2014).
 - [15] M. Montinaro, G. Wüst, M. Munsch, Y. Fontana, E. Russo-Averchi, M. Heiss, A. F. i. Morral, R. J. Warburton, and M. Poggio, *Nano Lett.* **14**, 4454 (2014).
 - [16] M. Munsch, A. V. Kuhlmann, D. Cadeddu, J.-M. Gérard, J. Claudon, M. Poggio, and R. J. Warburton, *Nat. Commun.* **8**, 76 (2017).
 - [17] E. R. MacQuarrie, T. A. Gosavi, N. R. Jungwirth, S. A. Bhawe, and G. D. Fuchs, *Phys. Rev. Lett.* **111**, 227602 (2013).
 - [18] P. Ouartchaiyapong, K. W. Lee, B. A. Myers, and A. C. Bleszynski Jayich, *Nat. Commun.* **5**, 4429 (2014).
 - [19] G. Balasubramanian, P. Neumann, D. Twitchen, M. Markham, R. Kolesov, N. Mizuochi, J. Isoya, J. Achard, J. Beck, J. Tissler, V. Jacques, P. R. Hemmer, F. Jelezko, and J. Wrachtrup, *Nat. Mater.* **8**, 383 (2009).
 - [20] A. Gruber, A. Dräbenstedt, C. Tietz, L. Fleury, J. Wrachtrup, and C. v. Borczyskowski, *Science* **276**, 1202 (1997).
 - [21] P. Ouartchaiyapong, L. M. A. Pascal, B. A. Myers, P. Lauria, and A. C. Bleszynski Jayich, *Appl. Phys. Lett.* **101**, 163505 (2012).
 - [22] Y. Tao and C. Degen, *Adv. Mater.* **25**, 3962 (2013).
 - [23] Y. Tao, J. M. Boss, B. A. Moores, and C. L. Degen, *Nat. Commun.* **5**, 3638 (2014).
 - [24] P. Rabl, S. J. Kolkowitz, F. H. L. Koppens, J. G. E. Harris, P. Zoller, and M. D. Lukin, *Nat. Phys.* **6**, 602 (2010).
 - [25] S. J. M. Habraken, K. Stannigel, M. D. Lukin, P. Zoller, and P. Rabl, *New J. Phys.* **14**, 115004 (2012).
 - [26] K. V. Keesidis, S. D. Bennett, S. Portolan, M. D. Lukin, and P. Rabl, *Phys. Rev. B* **88**, 064105 (2013).
 - [27] G. Davies and M. F. Hamer, *Proc. R. Soc. London, Ser. A* **348**, 285 (1976).
 - [28] J. Teissier, A. Barfuss, P. Appel, E. Neu, and P. Maletinsky, *Phys. Rev. Lett.* **113**, 020503 (2014).
 - [29] P. Tamarat, N. B. Manson, J. P. Harrison, R. L. McMurtrie, A. Nizovtsev, C. Santori, R. G. Beausoleil, P. Neumann, T. Gaebel, F. Jelezko, P. Hemmer, and J. Wrachtrup, *New J. Phys.* **10**, 045004 (2008).
 - [30] A. Batalov, V. Jacques, F. Kaiser, P. Siyushev, P. Neumann, L. J. Rogers, R. L. McMurtrie, N. B. Manson, F. Jelezko, and J. Wrachtrup, *Phys. Rev. Lett.* **102**, 195506 (2009).
 - [31] L. J. Rogers, S. Armstrong, M. J. Sellars, and N. B. Manson, *New J. Phys.* **10**, 103024 (2008).
 - [32] M. W. Doherty, V. V. Struzhkin, D. A. Simpson, L. P. McGuinness, Y. Meng, A. Stacey, T. J. Karle, R. J. Hemley, N. B. Manson, L. C. L. Hollenberg, and S. Prawer, *Phys. Rev. Lett.* **112**, 047601 (2014).
 - [33] L. J. Rogers, M. W. Doherty, M. S. J. Barson, S. Onoda, T. Ohshima, and N. B. Manson, *New J. Phys.* **17**, 013048 (2015).
 - [34] I. Wilson-Rae, P. Zoller, and A. Imamoglu, *Phys. Rev. Lett.* **92**, 075507 (2004).
 - [35] P. Rabl, P. Cappellaro, M. V. G. Dutt, L. Jiang, J. R. Maze, and M. D. Lukin, *Phys. Rev. B* **79**, 041302(R) (2009).
 - [36] P. Rabl, *Phys. Rev. B* **82**, 165320 (2010).
 - [37] S. Meesala, Y.-I. Sohn, H. A. Atikian, S. Kim, M. J. Burek, J. T. Choy, and M. Lončar, *Phys. Rev. Appl.* **5**, 034010 (2016).
 - [38] E. R. MacQuarrie, M. Otten, S. K. Gray, and G. D. Fuchs, *Nat. Commun.* **8**, 14358 (2017).
 - [39] A. Barfuss, J. Teissier, E. Neu, A. Nunnenkamp, and P. Maletinsky, *Nat. Phys.* **11**, 820 (2015).

- [40] E. R. MacQuarrie, T. A. Gosavi, A. M. Moehle, N. R. Jungwirth, S. A. Bhave, and G. D. Fuchs, *Optica* **2**, 233 (2015).
- [41] E. R. MacQuarrie, T. A. Gosavi, S. A. Bhave, and G. D. Fuchs, *Phys. Rev. B* **92**, 224419 (2015).
- [42] J. Teissier, A. Barfuss, and P. Maletinsky, *J. Opt.* **19**, 044003 (2017).
- [43] M. S. J. Barson, P. Peddibhotla, P. Ovarthaiyapong, K. Ganesan, R. L. Taylor, M. Gebert, Z. Mielens, B. Koslowski, D. A. Simpson, L. P. McGuinness, J. McCallum, S. Praver, S. Onoda, T. Ohshima, A. C. Bleszynski Jayich, F. Jelezko, N. B. Manson, and M. W. Doherty, *Nano Lett.* **17**, 1496 (2017).
- [44] F. Grazioso, B. R. Patton, P. Delaney, M. L. Markham, D. J. Twitchen, and J. M. Smith, *Appl. Phys. Lett.* **103**, 101905 (2013).
- [45] K. W. Lee, D. Lee, P. Ovarthaiyapong, J. Minguzzi, J. R. Maze, and A. C. Bleszynski Jayich, *Phys. Rev. Appl.* **6**, 034005 (2016).
- [46] P. Udvarhelyi, V. O. Shkolnikov, A. Gali, G. Burkard, and A. Pályi, *Phys. Rev. B* **98**, 075201 (2018).
- [47] A. E. Hughes and W. A. Runciman, *Proc. Phys. Soc.* **90**, 827 (1967).
- [48] E. Kaxiras, *Atomic and Electronic Structure of Solids* (Cambridge University Press, Cambridge, UK, 2003).
- [49] R. Gross and A. Marx, *Festkörperphysik* (De Gruyter Oldenbourg, Berlin, Boston, 2012).
- [50] See Supplemental Material at <http://link.aps.org/supplemental/10.1103/PhysRevB.99.174102> for a *Mathematica* file containing details of our calculations.
- [51] M. M. Mehrabadi, S. C. Cowin, and J. Jaric, *Int. J. Solids Struct.* **32**, 439 (1995).
- [52] T. Nagel, U.-J. Görke, K. M. Moerman, and O. Kolditz, *Environ. Earth Sci.* **75**, 937 (2016).
- [53] I. K. Ludlow, *J. Phys. C* **1**, 1194 (1968).
- [54] R. T. Fenner and J. N. Reddy, *Mechanics of Solids and Structures* (CRC, Boca Raton, 2012).
- [55] I. H. Shames and F. A. Cozzarelli, *Elastic and Inelastic Stress Analysis* (Prentice-Hall, Englewood Cliffs, NJ, 1992).
- [56] A. N. Cleland, *Foundations of Nanomechanics: From Solid-State Theory to Device Applications* (Springer-Verlag, Berlin, Heidelberg, 2003).
- [57] W. Voigt, *Lehrbuch der Kristallphysik* (Vieweg+Teubner Verlag, Berlin, 1966).